Published in final edited form as:
Brain Res. 2007 May 7; 1148: 1–14.

Mutational Analysis of Aspartoacylase: Implications for Canavan Disease

Jeremy R. Hershfield[*], **Nagarajan Pattabiraman**[‡], **Chikkathur N. Madhavarao**[*], and **M.A. Aryan Namboodiri**[*]

***** *Department of Anatomy, Physiology and Genetics, Uniformed Services University of the Health Sciences, Bethesda, Maryland, 20814*

‡ *Department of Oncology, Lombardi Comprehensive Cancer Center, Georgetown University, Washington, DC 20057*

Abstract

Mutations that result in undetectable activity of aspartoacylase, which catalyzes the deacetylation of *N*-acetyl-L-aspartate, correlate with Canavan Disease, a neurodegenerative disorder usually fatal during childhood. The underlying biochemical mechanisms of how these mutations ablate activity are poorly understood. Therefore, we developed and tested a three-dimensional homology model of aspartoacylase based on zinc dependent carboxypeptidase A. Mutations of the putative zinc-binding residues (H21G, E24D/G, and H116G), the general proton donor (E178A), and mutants designed to switch the order of the zinc-binding residues (H21E/E24H and E24H/H116E) yielded wild-type aspartoacylase protein levels and undetectable ASPA activity. Mutations that affect substrate carboxyl binding (R71N) and transition state stabilization (R63N) also yielded wild-type aspartoacylase protein levels and undetectable aspartoacylase activity. Alanine substitutions of Cys124 and Cys152, residues indicated by homology modeling to be in close proximity and in the proper orientation for disulfide bonding, yielded reduced ASPA protein and activity levels. Finally, expression of several previously tested (E24G, D68A, C152W, E214X, D249V, E285A, and A305E) and untested (H21P, A57T, I143T, P183H, M195R, K213E/G274R, G274R, and F295S) Canavan Disease mutations resulted in undetectable enzyme activity, and only E285A and P183H showed wild-type aspartoacylase protein levels. These results show that aspartoacylase is a member of the caboxypeptidase A family and offer novel explanations for most loss-of-function aspartoacylase mutations associated with Canavan Disease.

Keywords

aspartoacylase; homology modeling; carboxypeptidase; Canavan Disease; aminoacylase; zinc metalloproteases; *N*-acetyl-aspartate; NAA

1. Introduction

Canavan Disease (CD) is a neurodegenerative disorder most prevalent among Ashkenazi Jews that is linked to mutations in the gene encoding aspartoacylase (EC 3.5.1.15; abb. ASPA),

Address correspondence to: M.A. Aryan Namboodiri, Department of Anatomy Physiology and Genetics, USUHS, 4301 Jones Bridge Rd, Bethesda, MD 20814, Tel. 301 295-9357; Fax. 301 295-3566; E-Mail: anamboodiri@usuhs.mil

which catalyzes deacetylation of *N*-acetyl-L-aspartate (NAA). Typical CD pathology is marked by early onset macrocephaly, head-lag, ataxia, severe psychomotor retardation, brain vacuolization, and dysmyelination resulting in death during childhood, though there are several reports of clinically protracted disease courses (Elpeleg *et al.* 1994,Janson *et al.* 2006,Leone *et al.* 1999,Matalon *et al.* 1995,Matalon *et al.* 1988,Shaag *et al.* 1995,Surendran *et al.* 2003a,Tacke *et al.* 2005,Yalcinkaya *et al.* 2005,Zafeiriou *et al.* 1999,Zelnik *et al.* 1993). Considerable effort has been devoted to understanding the basis of CD by elucidating the function of ASPA in the central nervous system (CNS). Developmental increases in ASPA and NAA correlate with myelination (Burri *et al.* 1991,D'Adamo *et al.* 1968,D'Adamo *et al.* 1973,Kirmani *et al.* 2003) and several studies have shown incorporation of acetate from NAA into myelin lipids (Benuck & D'Adamo 1968,Burri et al. 1991,Chakraborty *et al.* 2001,D'Adamo & Yatsu 1966,Mehta & Namboodiri 1995). Total acetate levels and complete myelin lipid synthesis have recently been shown to be deficient in brains of CD knockout mice (Madhavarao et al. 2005), providing strong support for the hypothesis that NAA in the CNS supplies acetyl groups for lipid synthesis during myelination (Hagenfeldt *et al.* 1987,Kirmani *et al.* 2002,Kirmani et al. 2003,Madhavarao et al. 2005,Mehta & Namboodiri 1995). Furthermore, ASPA is found in cells within both cytoplasm and nucleus (Hershfield et al. 2006), though its role in the nucleus is yet to be delineated. There are few reports, however, that describe the mechanistic reason for the loss of ASPA activity due to certain mutations.

Currently, there are at least 56 mutations in the ASPA gene that correlate with CD, including 44 missense and nonsense mutations (Stenson *et al.* 2003,Zeng *et al.* 2006). Among Ashkenazi Jews, the E285A mutation is the most common (Elpeleg et al. 1994,Feigenbaum *et al.* 2004,Kaul *et al.* 1994,Kaul *et al.* 1996,Kronn *et al.* 1995), and the A305E mutation is the most common one among other populations (Elpeleg & Shaag 1999,Janson et al. 2006,Kaul et al. 1994,Kaul et al. 1996,Shaag et al. 1995,Sistermans *et al.* 2000,Yalcinkaya et al. 2005,Zeng et al. 2006,Zeng *et al.* 2002). Less than half of the missense mutations in the ASPA gene have been shown to yield negligible ASPA activity compared with wild-type (WT) enzyme upon transient transfection into COS cells. It is unknown whether CD mutations result in a loss of ASPA protein or a loss of catalytic function.

Although its functional domains remain uncharacterized, ASPA has been referred to as a member of the α/β-hydrolase superfamily of enzymes because of its enzymatic inhibition by diisopropyl fluorophosphates, which suggests a catalytic serine, and because of its local sequence homology to catalytic cores in esterases (Cygler *et al.* 1993,Kaul *et al.* 1993,Matalon & Michals-Matalon 1999). However, ASPA lacks an invariant serine, a candidate for a catalytic residue, and an alignment study revealed minimal homology of ASPA with serine proteases (Makarova & Grishin 1999,Cygler et al. 1993).

On the other hand, this same alignment study indicated that ASPA is structurally similar to members of the zinc carboyxpeptidase family (Makarova & Grishin 1999). Consistent with this possibility, divalent cation chelators drastically reduced ASPA activity in bovine brain homogenates and in dialyzed recombinant human ASPA from *E. coli* (Le Coq et al. 2006) (Kaul *et al.* 1991,Moore *et al.* 2003). Zinc chloride slightly increased purified bovine brain ASPA activity at low concentrations and inhibited activity at higher concentrations (Kaul et al. 1991). Roughly two atoms of zinc were detected per enzyme subunit following dialysis and denaturation of recombinant human ASPA expressed in *E. coli*, though zinc-treated ASPA had the same activity as the native enzyme refolded without additional metal ions (Moore et al. 2003). These results collectively suggest that ASPA is a metalloenzyme, but the effects of zinc on its catalytic activity remain unclear.

The three-dimensional structure of ASPA, or any other aminoacylase, is currently unknown. Conversely, there are numerous structures of zinc-dependent carboxypeptidase family

members (Jensen *et al.* 2002,Rees *et al.* 1983,Bukrinsky *et al.* 1998,Christianson & Lipscomb 1986,Shoham *et al.* 1984). Several residues in bovine zinc-dependent carboxypeptidase A (EC 3.4.17.1; abb. ZnCPA) that are critical to the catalytic mechanism are conserved in human and murine ASPA (Makarova & Grishin 1999,Namboodiri *et al.* 2000). These include residues that are equivalent to those involved in zinc coordination (His21, Glu24, His116), shaping the substrate-binding cavity (Asp68), substrate binding (Arg71), transition state stabilization (Arg63), and catalysis (Glu178) (Makarova & Grishin 1999). Notably, missense mutations at His21, Glu24, Asp68, and Arg71 have been detected in CD patients (Sistermans et al. 2000,Zeng et al. 2002,Janson et al. 2006). Although there are no CD mutations at Glu178, nearby CD mutations have been found at Pro181, Pro183, and Val186 (Sistermans et al. 2000,Zeng et al. 2002,Elpeleg & Shaag 1999), which suggests that Glu178 is an important catalytic residue.

To test the hypothesis that ASPA is a zinc-dependent metalloenzyme, as well as to address the biochemical basis for undetectable ASPA activity in several CD-associated ASPA mutations, we have generated and evaluated a 3D homology-based active/binding site model of ASPA based on ZnCPA. Specifically, CD-associated ASPA missense mutations in this report include those that appear frequently in the literature (G274R, F295S, E285A, A305E), affect a putative active site residue (H21P, E24G, A57T, D68A), or assist in spaning the complete ASPA cDNA (I143T, C152W, P183H, M195R, K213E, D249V). In addition, we analyzed a K213E/G274R double mutation that has been associated with a mild phenotype of CD (Tacke et al. 2005).

2. Results

2.1. Homology-Based Modeling of ASPA

The BLAST program was used to identify sequences close to the human ASPA (Swiss-Prot Identity P45381 (http://www.expasy.org/uniprot/P45381#seq)) sequence in the PDB structures, yielding the x-ray structure of Succinylglutamate Desuccinylase from *Vibrio parahaemolyticus* as the highest scoring structure. However, careful analysis of this alignment showed there was no alignment for the third zinc-binding ligand. Therefore, the complete active site of ASPA could not be constructed using the succinylglutamate desuccinylases. On the other hand, alignments of the human ASPA sequence against carboxypeptidase A, carboxypeptidase G, and aminopeptidase have recently been reported (Makarova & Grishin 1999). Two zinc ions were reported to bind to aminopeptidase (Berman *et al.* 2000,Chevrier *et al.* 1994) and carboxypeptidase G2 (Berman et al. 2000,Rowsell *et al.* 1997). In these peptidases, the ligands were shared between the two zinc ions. In carboxypeptidase A, however, only one zinc ion is bound to the enzyme because the Glu ligand required for binding the second zinc ion has been replaced by Phe (Makarova & Grishin 1999). Similarly, the region containing this glutamate is absent in the human ASPA sequence. Therefore, sequence alignment and homology modeling indicate that the human ASPA enzyme likely binds a single zinc atom.

A partial homology model of ASPA (ACY2_human) was generated using the reported coordinates for the crystal structure of bovine (*Bos taurus*) pancreas ZnCPA (PDB Code 8CPA) at a resolution of 2 Å (Berman et al. 2000,Kim & Lipscomb 1991) and the reported alignment between human ASPA and ZnCPA (Makarova & Grishin 1999). The sequence alignment between human ASPA and ZnCPA used in this paper is shown in Figure 1. As there were several gaps between ASPA and ZnCPA in this alignment, a fragment-based alignment approach was used to build a homology model containing the critical residues in and around the active site. The gaps denoted by the number in the square brackets have been carefully checked with the crystal structure of 8CPA in order to smoothly align the sequence fragments.

The presentation and assessment of the final homology model for ASPA are shown in Figure 2. The protein is represented by ribbons and the potentially critical catalytic and substrate

binding residues in the active site, His21, Glu24, His116, Glu178, Arg63, and Arg71, are shown by atom color-coded ball and stick representation (Fig. 2A). A zinc atom (shown by cyan sphere) that is coordinated by His21, His116 and Glu24 is also shown. In addition, the four cysteine residues of ASPA, Cys61, Cys67, Cys124, and Cys152, which are discussed in this report, are also depicted using ball and stick. The Ramachandran plot for the residues of the homology model is depicted in Figure 2B. Almost all of the residues fall within the energetically allowed region of the plot. Therefore, the homology model does not have any unwanted non-bonded contacts.

Although the homology model of ASPA does not include the N-terminal 60 amino acid residues of the carboxypeptidase, the catalytic residues of the active sites correspond very well. ASPA and ZnCPA both catalyze the hydrolysis of a C-terminal peptide bond (Fig. 3A) and there is a close superposition of the catalytic residues of the ASPA homology model (bonds shown by lines) onto the ZnCPA structure (bonds by thick lines and labeled) (Fig. 3B).

2.2. Characterization of Zinc-Coordination and ASPA Catalysis

Our partial 3D homology model suggests several residues that could potentially be involved in NAA binding and/or hydrolysis. The rationale for all of the mutations analyzed in this report is summarized in Table 1. Consistent with the previous methodology for *in vitro* analysis of CD-associated ASPA mutations, extracts of transiently transfected COS-7 cells were analyzed for ASPA activity.

Mutation of the conserved residues corresponding to bovine CPA's three zinc-binding ligands (His21, Glu24, His116) and general proton donor (Glu178), to alanine or glycine yielded WT levels of ASPA protein by immunoblotting with pepASPA (Fig. 4A) and undetectable ASPA activity by a high-sensitivity radiometric ASPA assay (Madhavarao et al. 2002) (Fig. 4B) [see Fig. 7A for E24G]. Double mutants that switched the order of the putative zinc-binding ligands (H21E/E24H and E24H/H116E; Fig. 4C) also yielded catalytically defective enzymes.

The mutation of glutamate to aspartate, which shortens the length of the putative zinc ligand by ~1.5 Å, at residue 24 resulted in a catalytically defective enzyme (Fig. 4B). Although aspartate can be a zinc ligand (Le Moual *et al.* 1991,Medina *et al.* 1991,Vallee & Auld 1990b,Vallee & Auld 1990a), it does not appear to function this way in ASPA. The E24D mutation in ASPA showed no detectable activity from either crude COS-7 cell extract or when partially purified using nickel-affinity chromatography of a C-terminal V5-His tag (data not shown).

Finally, arginines which roughly align with those that bind the C-terminal carboxyl group of the substrate (Arg145→Arg71) and stabilize the gem diolate anion intermediate (Arg127→Arg63) in bovine ZnCPA (Makarova & Grishin 1999) were mutated to asparagines to maintain local geometry and lose a positive charge. Expression of the R71N and R63N mutations yielded WT ASPA protein levels (Fig. 4A) and undetectable ASPA activity (Fig. 4B).

Because there is very little ASPA protein in crude extracts of transiently transfected COS-7 cells, it is possible that certain mutations which yield undetectable activity in COS cells might yield residual activity using more enzyme. Therefore, we expressed and purified from *E. coli* mutations of the putative zinc-binding ligands to explore this possibility. One-step nickel-affinity chromatography partial purification of WT, H21G, E24D, E24G, and H116G yielded single bands at ~52 kDa, corresponding to the molecular weight of native ASPA plus the 13 kDa thioredoxin N-terminal fusion protein and the 3 kDa C-terminal tags (Fig. 5). There was undetectable ASPA activity from each purified mutant using 10–15 μg of protein in the spectrophotometric ASPA assay (see Materials and Methods). Under the same assay conditions

with ~5 μg of the purified WT enzyme the substrate was almost completely catalyzed, as in previous experiments (Moore et al. 2003,Namboodiri et al. 2000).

2.3. Role of Cysteines in ASPA

Our partial homology model (Fig. 2) depicts the four cysteine residues in ASPA. Mutations at Cys152 have been associated with CD and yield undetectable ASPA activity upon *in vitro* expression in COS cells (Kaul et al. 1996,Kaul *et al.* 1995,Zeng et al. 2002). Also, low concentrations of DTT are required to maintain ASPA activity, whereas high concentrations ablate activity (Kaul et al. 1991,Madhavarao et al. 2002). Therefore, it has been suggested that there is an intramolecular disulfide bond in ASPA involving Cys152. Assuming that ASPA lacks the overall flexibility necessary for distal disulfide bonds, only the proximal cysteine pairs can form disulfide bridges *in vivo*. Our homology model indicates that Cys124 and Cys152, but not Cys61 and Cys67, are correctly orientated for disulfide bonding.

We analyzed the potential of Cys124 and Cys152 to disulfide bond using small, sterically non-interfering alanine substitutions (Fig. 6). Cys61 was included in our analysis because it had been previously suggested to bind to Cys152 (Kaul et al. 1995) and because it is near the putative active site. We also generated a serine substitution at Cys61 to mimic the possibility of the sulfhydryl group participating in catalysis via a proton donor/acceptor mechanism. Immunoblotting showed WT ASPA protein levels for C61A and C61S and diminished levels for C124A and C152A (Fig. 6A). Based on the relative amounts of ASPA protein, C61A and C61S yielded WT ASPA activity and C124A and C152A yielded about 50% of WT activity (Fig. 6B). Similar to how a bulky tryptophan substitution at Cys152 might destabilize the ASPA protein (see Fig. 7A), C61W was adequately transcribed (Fig. 7B, top panel), but resulted in a nearly complete absence of ASPA protein and activity (Fig. 6).

2.4. Protein Characteristics of CD Mutant ASPA

We next evaluated the ASPA homology model using biologically relevant CD mutations that span the entire ASPA gene (Table 2). It has been hypothesized that many non-conservative CD mutants exert deleterious effects due to a loss of structural integrity by a drastic conformational change, rather than directly disrupting catalytic events at the active site (Moore et al. 2003,Shaag et al. 1995,Zeng et al. 2002). Therefore, CD mutations resulting in nearly WT ASPA protein levels likely suggest defective catalysis, while those drastically decreasing ASPA protein suggest something other than defective catalysis.

We first analyzed a subset of missense mutations in the ASPA gene that were previously shown to result in undetectable enzyme activity upon *in vitro* expression. For each of these six mutants, comparable levels of ASPA mRNA, when normalized to a loading control, were detected by RT-PCR (Fig. 7A, top panel). Immunoblotting for ASPA protein showed strong reductions for C152W, D249V, and A305E, mild reductions for E24G and D68A, and WT levels for E285A (Fig. 7A, middle panel). The E214X truncation mutant was used as a negative control for detection of full-length ASPA at ~36 kDa. Finally, we confirmed that E24G, D68A, C152W, E214X, D249V, E285A, and A305E each yield undetectable ASPA activity (Kaul et al. 1994,Zeng et al. 2002) compared to ~20 nmol/h/mg protein specific activity for WT ASPA (Fig. 7A, bottom panel).

We next analyzed a subset of missense mutations in the ASPA gene that were diagnostically linked to CD but not tested *in vitro.* For each of these eight mutants, comparable levels of ASPA mRNA, when normalized to a loading control, were detected by RT-PCR (Fig. 7B, top panel). Immunoblotting showed a nearly complete absence of ASPA protein for H21P, I143T, and F295S, strong reductions for M195R and G274R, a mild reduction for A57T, and WT levels for P183H and K213E (Fig. 7B, middle panel). Finally, there was WT activity for K213E,

~5% residual activity for G274R, and undetectable activity for H21P, A57T, I143T, P183H, M195R, and F295S (Fig. 7B, bottom panel). Indicative of a silent mutation, the reversal of charge at Lys213 did not affect ASPA activity, which suggests that Lys213 is not crucial for catalytically active ASPA protein.

Lastly, in a recent case report, K213E was postulated to serve a protective role in promoting a mild clinical phenotype of CD as a double mutation with G274R (Tacke et al. 2005). To explore this possibility, we generated and analyzed the K213E/G274R double mutant and found that it results in a nearly complete absence of ASPA protein (Fig. 7C, top panel) and activity (Fig. 7C, bottom panel). Therefore, it does not appear to be different from G274R, which also yielded reduced ASPA protein and activity levels.

3. Discussion

In our current report, we explored the possibility that ASPA is a member of the zinc-peptidase superfamily of enzymes (Makarova & Grishin 1999) by generating an active/binding site model for ASPA based on homology to ZnCPA. Mutational analysis of residues that are potentially involved in zinc coordination (His21, Glu24, His116), general proton donation (Glu178), substrate carboxyl binding (Arg71), and transition state stabilization (Arg63) suggests they are critical for ASPA catalysis. Mutational analysis also suggests that ASPA activity and stability might depend on an intramolecular disulfide bond between Cys124 and Cys152. The analysis of several ASPA mutations that are clinically associated with CD suggests that E24G, A57T, D68A, P183H, and E285A are catalytic mutations; H21P, I143T, C152W, M195R, D249V, F295S, and A305E are non-catalytic mutations; and K213E does not play a protective role in promoting a mild CD phenotype.

Mutations of ASPA residues equivalent to ZnCPA's zinc ligands (His21, Glu24, and His116), general proton donor (Glu178), substrate-binding determinant (Arg71), and substrate-cavity shaping residue (Asp68) result in catalytically defective ASPA protein. Analysis of the E24D mutation suggests that shortening the side chain by a single C-C bond drastically alters zinc binding that might polarize the zinc-coordinated water molecule for catalysis (Laustsen *et al.* 2001,Le Moual et al. 1991). Although highly conserved Glu→Asp mutations have resulted in weakened zinc affinity and a lowered K_m in similar enzymes (Le Moual et al. 1991,Vazeux *et al.* 1996), we could not detect residual ASPA activity for the E24D mutant. While the E24G mutant could have resulted in a loss of activity due to structural differences, the conserved E24D mutant still displayed a loss of activity, suggesting that this glutamate is directly involved in catalysis (Vazeux et al. 1996). In addition, the order of the three metal binding ligands was found to be crucial for zinc-promoted enzymatic catalysis. This is consistent with the notion that identity, spacing, and secondary interactions with neighboring amino acids are all crucial for zinc-mediated catalysis (Auld 2001).

The data in this report suggest that ASPA follows a catalytic mechanism similar to that of ZnCPA (Fig. 8) (Jensen et al. 2002,Wouters & Husain 2001). Using ZnCPA-bound ligand inhibitor crystal structures as a template (Jensen et al. 2002), we propose that Arg71 binds the carboxylate group of the NAA, while the acetyl group is fitted into the active site by its affinity towards the zinc atom (Fig. 8A). At this stage, the zinc ion is five coordinated: Glu24 bidentate, His21, His116, and a water molecule (Vallee & Auld 1990b,Vallee & Auld 1990a). The oxygen of the scissile carbonyl now interacts with zinc and forms its sixth ligand. Along with the approaching guanidine group of Arg63, this interaction helps zinc to activate the water ligand and further polarize the scissile carbonyl group (Kim & Lipscomb 1990). Acidic zinc-activated water can then donate a proton to Glu178 and create a zinc-bound hydroxy anion which performs a nucleophilic attack on the scissile carbonyl carbon of the acetyl group of NAA (Fig. 8B). The resulting transition state is a gem-diolate anion that is stabilized by its interactions

with the guanidinium group of Arg63, zinc, and the carboxyl side chain of Glu178 (Fig. 8C). Our mutational analysis is consistent with the hypothesis that the positive charge of Arg63 is required to favor the formation and stabilization of the transition state. The inevitable collapse of the transition state results in the formation of aspartate and acetate from NAA as Glu178 provides the proton required to form the primary amino group of aspartate. The hydrolysis of NAA concludes as the hydroxyl group from water becomes part of acetate and the proton becomes part of the primary amino group of aspartate (Fig. 8D). Electrostatic repulsions of the acetate and aspartate products with active site side chains likely facilitate their release from ASPA (Fig. 8D).

The assumptions in the literature pertaining to ASPA's catalytic mechanism are consistent with this proposed catalytic mechanism. The carbon backbone of NAA has been suggested to interact with ASPA's active site because substrates with more electronegative carbonyl groups are better substrates for ASPA-mediated hydrolysis (Matalon *et al.* 1993,Kaul et al. 1991). A nucleophilic attack is then believed to occur at the carbonyl group, irrespective of the α and β-carboxyl groups (Moore et al. 2003).

Most mutations in this report yielded undetectable ASPA activity using a TLC-based assay and a fixed concentration of NAA near the published K_M value (Namboodiri et al. 2000). Previous reports using different ASPA enzyme assays sometimes detected residual activity for various CD-associated ASPA mutations, likely as a result of longer enzyme-substrate incubations, higher substrate concentrations, and inherent background activity that is absent from the TLC-based assay (Madhavarao et al. 2002).

With a partial homology model and a hypothetical catalytic mechanism for ASPA-mediated NAA hydrolysis, we can offer explanations for how several CD-associated mutations result in a loss of activity *in vivo*. The E24G mutation precludes zinc-binding and the A57T and D68A mutations disrupt the substrate binding cavity. The mutation of a proline at residue 183, which is the site of a type I reverse turn (Pro282) in ZnCPA (Makarova & Grishin 1999), removes a bend that is crucial for local geometry and misaligns the putative catalytic residue, Glu178. The molecular basis of the E285A mutation remains unclear, though our data corroborate its putative catalytic role (Kaul et al. 1993), rather than a more recently proposed loss of protein integrity attributed to Ala and Asp substitutions at Glu285 (Moore et al. 2003). Our homology model of ASPA does not include the first 60 amino acids of ZnCPA, which appear to stabilize a part of the substrate binding pocket. Therefore, one possibility is that ASPA's C-terminus might replace these 60 amino acids of ZnCPA and stabilize ASPA's substrate binding pocket. All other CD-associated ASPA mutations investigated in this report—including H21P, I143T, C152W, M195R, D249V, G274R, and A305E—appear to disrupt non-catalytic aspects of ASPA protein through the introduction of a turn (H21P), the loss of hydrophobicity (I143T, M195R, G274R and A305E), the introduction of a bulky residue (C152W), or the loss of charge (D249V). The nature of these protein defects remains unclear.

Importantly, the resulting catalytic or non-catalytic protein phenotype of a CD-associated ASPA mutation does not appear to correlate with a physiological phenotype. This is in contrast to a previous suggestion that active site mutations result in a severe phenotype (Surendran *et al.* 2003b). The most common mutation among non-Ashkenazi Europeans, A305E (non-catalytic), has been implicated in severe, classical, and mild CD cases (Janson et al. 2006,Shaag et al. 1995,Sistermans et al. 2000,Yalcinkaya et al. 2005). Similarly, the most common mutation among Ashkenazim, E285A (catalytic), has also been implicated in multiple CD clinical courses (Shaag et al. 1995).

In conclusion, we have used extensive mutational analysis to evaluate an active site homology model and show that ASPA likely follows a catalytic mechanism similar to ZnCPA. During

the preparation of this manuscript, a report was published which confirms our proposal that ASPA contains a single zinc atom (Le Coq et al. 2006). When this manuscript was in the process of review, the X-ray crystal structures of rat and human ASPA were published (Bitto et al. 2007). Upon comparing our homology model of the active and binding sites of ASPA with those of the published crystal structure, the root-mean-square deviations between C_α atoms is 1.1 Å. Also, our predictions of a single zinc binding site and the zinc ligands are in complete agreement with the crystal structure. Finally, the distance between the sulfur atoms of Cys124 and Cys152 is 5. 5 Å (Bitto et al. 2007), which means they are close enough for the formation of a disulfide bridge. Future studies would benefit from the proposed homology model and proposed catalytic mechanism, as well as the available crystal structure for drug design with the goal of restoring ASPA activity in CD patients with catalytically deficient ASPA enzyme (Qiao et al. 2006).

4. Experimental Procedures

4.1. Homology Modeling of Aspartoacylase

The coordinates for the 3D model of human ASPA protein were generated using the homology-modeling program, Modeler (v. 6.2; http://salilab.org/modeller/). A single zinc ion was manually placed onto the homology model to favorably coordinate with His, Glu, and His. The homology model of ASPA with the zinc ion was then energy-minimized using constrained minimization and the molecular mechanics program, AMBER6 (http://amber.scripps.edu/). The molecular visualization program, Chimera (http://www.cgl.ucsf.edu/chimera/), was used to analyze the quality of the final homology model and generate the figures reported in this paper. Also, the backbone torsion angles, phi and psi for all residues of the homology model were checked against the energetically allowed regions of the Ramachandran Plot. (http://144.16.71.146/rp/index.html).

4.2. Plasmid Constructs and Site-Directed Mutagenesis

Full-length human ASPA cDNA was subcloned by polymerase chain reaction (PCR) using primers ATGACTTCTTGTCACATTGCT (forward) and CTAATGTAAACAGCAGCGAAT (reverse) from pBAD/Thio-TOPO (Invitrogen, Carlsbad, CA) (Namboodiri et al. 2000) into the TOPO-T/A cloning site of pcDNA3.1/V5-His-TOPO such that the resulting hASPA plasmid expresses untagged, native ASPA. Individual point mutations were introduced into native untagged hASPA using Stratagene's Quick Change II Site-Directed Mutagenesis Kit (La Jolla, CA) according to manufacturer's instructions (Table 3). Mutant plasmid DNA was then isolated and sequenced to confirm the desired mutation. For bacterial expression, mutants were generated directly in the pBAD/Thio-TOPO vector such that the resulting hASPA-V5-His plasmid expresses ASPA with thioredoxin at its N-terminus and a V5 epitope and a (6x)-histidine domain at its C-terminus.

4.3. Cell Culture and Transient Transfections

COS-7 (ATCC, Manassas, VA) cells were grown at 37°C with 5% CO_2 in Dulbecco's modified Eagle Medium (DMEM) containing 10% fetal bovine serum (FBS). Transient transfections were performed using Lipofectamine 2000 (Invitrogen) with 1.2 μg plasmid DNA added to 90% confluent cells in 12-well plates. COS-7 cells were harvested 24 h post-transfection by treatment with 2 mM EDTA (10 min, 37°C), spun down, and washed with phosphate buffered saline (PBS). Whole cell extracts were prepared by sonicating cell pellets in homogenization buffer (0.5 mM DTT, 50 mM Tris-HCl, pH 8.0, 50 mM NaCl, 0.05% IGEPAL CA-630, 10% glycerol). Cellular debris was then removed (16,000 *g*, 10 min, 4°C) and protein concentrations were determined using Bio-Rad's DC protein assay (Hercules, CA).

4.4. Bacterial Expression and Nickel-Affinity Chromatography

Bacterial expression and nickel affinity chromatography were followed as previously described (Namboodiri et al. 2000). Briefly, 5 ml of Luria–Bertani medium containing ampicillin (100 μg/ml) was inoculated with a single recombinant *E. coli* colony and incubated overnight at 37° C with shaking (225–250 rpm) to OD_{600} = 1.0–2.0. The culture medium was then used to inoculate 2 L of LB medium containing ampicillin (100 μg/ml), and the cells were grown at 37°C with shaking to an OD_{600} of about 0.5. Arabinose was added (0.2%) to induce the expression of ASPA and the cells were grown for 4.5 h. Bacterial pellets were harvested by centrifugation. The bacterial pellet was suspended in 50 ml of sodium phosphate (20 mM, pH 7.8) containing sodium chloride (500 mM), DTT (1 mM), IGEPAL CA630 (0.1%; Sigma, St. Louis, MO), 10% (w/v) glycerol and protease inhibitor cocktail (Sigma). The preparation was sonicated and centrifuged (13,000 *g*, 30 min, 4°C) and the supernatant was used for purification.

The affinity column (~10 ml bed volume) using ProBond resin (Invitrogen) was prepared by equilibrating with sodium phosphate (20 mM, pH 7.8) containing sodium chloride (500 mM) glycerol (10%, w/v) and DTT (1 mM), and the bacterial extract was gently mixed with the resin for 30 min. The column was then washed extensively with the equilibrating buffer followed by a wash buffer (sodium phosphate 20 mM, sodium chloride 500 mM, pH 6.0). ASPA was eluted batch-wise using increasing concentrations (50, 100, 200, and 500 mM) of imidazole dissolved in the wash buffer. ASPA activity in the eluate was determined by spectrophotometric assay. Fractions corresponding to the 200 mM imidazole elution contained maximum ASPA activity and were pooled and dialyzed for further analysis.

4.5. Aspartoacylase Enzyme Assays

A high-sensitivity radiometric assay involving TLC-based product separation and phosphor image-based quantification was followed as previously described (Madhavarao et al. 2002). ASPA activity in transiently transfected COS-7 cell extracts was determined with a fixed total NAA concentration of 0.454 mM. ASPA activity of bacterially-expressed purified proteins was determined using a coupled spectrophotometric ASPA activity assay based on β-NADH oxidation of ASPA-liberated aspartate (Fleming & Lowry 1966) as previously described (Hershfield et al. 2006). Enzyme was incubated for 2 h with 2 mM NAA substrate. The units of enzyme activity are nmol product per hour per mg of total protein (nmol/hr/mg).

4.6. SDS-PAGE and Immunoblotting

Whole cell extracts were subjected to SDS-PAGE and immunoblotting as previously described (Hershfield et al. 2006). Following blocking, membranes were cut in half at the 45 kDa marker of the High-Range Rainbow Molecular Weight Marker (Amersham, Piscatway, NJ). Super Fast diaminobenzidine substrate (Sigma) was used for colorimetric detection of separate immunoblot signals from a rabbit polyclonal antibody raised against a partial ASPA peptide (pepASPA) and a monoclonal β-tubulin (α-βT) antibody (Upstate, Charlottesville, VA). Roughly 50 μg of protein from COS-7 extract was loaded per well. For proteins purified from bacteria, SDS-PAGE was followed by Coomassie staining with Gelcode Blue (Pierce, Rockford, IL) according to manufacturer's instructions. Between 5 and 10 μg of partially purified protein was loaded per well.

4.7. Qualitative RT-PCR

Total RNA was extracted from COS-7 cells 24 h post-transfection using the RNAqueous 4PCR kit (Ambion, Austin, TX), treated with DNase I, concentrated, and quantified. Two-step reverse transcription with heat denaturation was then carried out using Ambion's RETROscript kit. The resulting cDNA was amplified by PCR using either ASPA-specific gene primers GGGTATAGAAGTTGGTCCTCA (forward) and CTAATGTAAACAGCAGCGAAT

(reverse), or positive control primers against the housekeeping gene rig/S15 (Ambion), and analyzed by 2% agarose gel electrophoresis.

4.8. Statistical Analysis

Enzyme activities are presented as means ± SEM. The differences between groups were analyzed by ANOVA followed by the least significant difference post-hoc test at a significance level of $p < 0.05$.

4.9. Chemical Structures

All chemical structures and reactions were drawn using the MDL ISIS Draw 2.5 (Elsevier MDL, San Ramon, CA) program.

Acknowledgements

The research was supported by grants from the NIH (R01, NS39387) and Jacob's Cure, New York, to M.A.A.N. The authors thank Dr. Tao-Yiao John Wu and Dr. John Moffett for critical reading of the manuscript.

References

Auld DS. Zinc coordination sphere in biochemical zinc sites. Biometals 2001;14:271–313. [PubMed: 11831461]

Benuck M, D'Adamo AF Jr. Acetyl transport mechanisms. Metabolism of N-acetyl-L-aspartic acid in the non-nervous tissues of the rat. Biochim Biophys Acta 1968;152:611–618. [PubMed: 5690485]

Berman HM, Westbrook J, Feng Z, Gilliland G, Bhat TN, Weissig H, Shindyalov IN, Bourne PE. The Protein Data Bank. Nucleic Acids Res 2000;28:235–242. [PubMed: 10592235]

Bitto E, Bingman CA, Wesenberg GE, McCoy JG, Phillips GN Jr. Structure of aspartoacylase, the brain enzyme impaired in Canavan disease. Proc Natl Acad Sci U S A 2007;104:456–461. [PubMed: 17194761]

Bukrinsky JT, Bjerrum MJ, Kadziola A. Native carboxypeptidase A in a new crystal environment reveals a different conformation of the important tyrosine 248. Biochemistry 1998;37:16555–16564. [PubMed: 9843422]

Burri R, Steffen C, Herschkowitz N. N-acetyl-L-aspartate is a major source of acetyl groups for lipid synthesis during rat brain development. Dev Neurosci 1991;13:403–411. [PubMed: 1809557]

Chakraborty G, Mekala P, Yahya D, Wu G, Ledeen RW. Intraneuronal N-acetylaspartate supplies acetyl groups for myelin lipid synthesis: evidence for myelin-associated aspartoacylase. J Neurochem 2001;78:736–745. [PubMed: 11520894]

Chevrier B, Schalk C, D'Orchymont H, Rondeau JM, Moras D, Tarnus C. Crystal structure of Aeromonas proteolytica aminopeptidase: a prototypical member of the co-catalytic zinc enzyme family. Structure 1994;2:283–291. [PubMed: 8087555]

Christianson DW, Lipscomb WN. X-ray crystallographic investigation of substrate binding to carboxypeptidase A at subzero temperature. Proc Natl Acad Sci U S A 1986;83:7568–7572. [PubMed: 3463986]

Cygler M, Schrag JD, Sussman JL, Harel M, Silman I, Gentry MK, Doctor BP. Relationship between sequence conservation and three-dimensional structure in a large family of esterases, lipases, and related proteins. Protein Sci 1993;2:366–382. [PubMed: 8453375]

D'Adamo AF Jr, Gidez LI, Yatsu FM. Acetyl transport mechanisms. Involvement of N-acetyl aspartic acid in de novo fatty acid biosynthesis in the developing rat brain. Exp Brain Res 1968;5:267–273. [PubMed: 5712694]

D'Adamo AF Jr, Smith JC, Woiler C. The occurrence of N-acetylaspartate amidohydrolase (aminoacylase II) in the developing rat. J Neurochem 1973;20:1275–1278. [PubMed: 4697888]

D'Adamo AF Jr, Yatsu FM. Acetate metabolism in the nervous system. N-acetyl-L-aspartic acid and the biosynthesis of brain lipids. J Neurochem 1966;13:961–965. [PubMed: 5927765]

Elpeleg ON, Anikster Y, Barash V, Branski D, Shaag A. The frequency of the C854 mutation in the aspartoacylase gene in Ashkenazi Jews in Israel. Am J Hum Genet 1994;55:287–288. [PubMed: 8037206]

Elpeleg ON, Shaag A. The spectrum of mutations of the aspartoacylase gene in Canavan disease in non-Jewish patients. J Inherit Metab Dis 1999;22:531–534. [PubMed: 10407784]

Feigenbaum A, Moore R, Clarke J, Hewson S, Chitayat D, Ray PN, Stockley TL. Canavan disease: carrier-frequency determination in the Ashkenazi Jewish population and development of a novel molecular diagnostic assay. Am J Med Genet 2004;124A:142–147.

Fleming MC, Lowry OH. The measurement of free and N-acetylated aspartic acids in the nervous system. J Neurochem 1966;13:779–783. [PubMed: 5928222]

Hagenfeldt L, Bollgren I, Venizelos N. N-acetylaspartic aciduria due to aspartoacylase deficiency--a new aetiology of childhood leukodystrophy. J Inherit Metab Dis 1987;10:135–141. [PubMed: 3116332]

Hershfield JR, Madhavarao CN, Moffett JR, Benjamins JA, Garbern JY, Namboodiri A. Aspartoacylase is a regulated nuclear-cytoplasmic enzyme. Faseb J 2006;20:2139–2141. [PubMed: 16935940]

Janson CG, Kolodny EH, Zeng BJ, et al. Mild-onset presentation of Canavan's disease associated with novel G212A point mutation in aspartoacylase gene. Ann Neurol 2006;59:428–431. [PubMed: 16437572]

Jensen F, Bukrinsky T, Bjerrum J, Larsen S. Three high-resolution crystal structures of cadmium-substituted carboxypeptidase A provide insight into the enzymatic function. J Biol Inorg Chem 2002;7:490–499. [PubMed: 11941507]

Kaul R, Casanova J, Johnson AB, Tang P, Matalon R. Purification, characterization, and localization of aspartoacylase from bovine brain. J Neurochem 1991;56:129–135. [PubMed: 1987315]

Kaul R, Gao GP, Aloya M, Balamurugan K, Petrosky A, Michals K, Matalon R. Canavan disease: mutations among Jewish and non-jewish patients. Am J Hum Genet 1994;55:34–41. [PubMed: 8023850]

Kaul R, Gao GP, Balamurugan K, Matalon R. Cloning of the human aspartoacylase cDNA and a common missense mutation in Canavan disease. Nat Genet 1993;5:118–123. [PubMed: 8252036]

Kaul R, Gao GP, Matalon R, Aloya M, Su Q, Jin M, Johnson AB, Schutgens RB, Clarke JT. Identification and expression of eight novel mutations among non-Jewish patients with Canavan disease. Am J Hum Genet 1996;59:95–102. [PubMed: 8659549]

Kaul R, Gao GP, Michals K, Whelan DT, Levin S, Matalon R. Novel (cys152 > arg) missense mutation in an Arab patient with Canavan disease. Hum Mutat 1995;5:269–271. [PubMed: 7599639]

Kim H, Lipscomb WN. Crystal structure of the complex of carboxypeptidase A with a strongly bound phosphonate in a new crystalline form: comparison with structures of other complexes. Biochemistry 1990;29:5546–5555. [PubMed: 2386784]

Kim H, Lipscomb WN. Comparison of the structures of three carboxypeptidase A-phosphonate complexes determined by X-ray crystallography. Biochemistry 1991;30:8171–8180. [PubMed: 1868092]

Kirmani BF, Jacobowitz DM, Kallarakal AT, Namboodiri MA. Aspartoacylase is restricted primarily to myelin synthesizing cells in the CNS: therapeutic implications for Canavan disease. Brain Res Mol Brain Res 2002;107:176–182. [PubMed: 12487123]

Kirmani BF, Jacobowitz DM, Namboodiri MA. Developmental increase of aspartoacylase in oligodendrocytes parallels CNS myelination. Brain Res Dev Brain Res 2003;140:105–115.

Kobayashi K, Tsujino S, Ezoe T, Hamaguchi H, Nihei K, Sakuragawa N. Missense mutation (I143T) in a Japanese patient with Canavan disease. Hum Mutat 1998;(Suppl 1):S308–309. [PubMed: 9452117]

Kronn D, Oddoux C, Phillips J, Ostrer H. Prevalence of Canavan disease heterozygotes in the New York metropolitan Ashkenazi Jewish population. Am J Hum Genet 1995;57:1250–1252. [PubMed: 7485179]

Laustsen PG, Vang S, Kristensen T. Mutational analysis of the active site of human insulin-regulated aminopeptidase. Eur J Biochem 2001;268:98–104. [PubMed: 11121108]

Le Coq J, An HJ, Lebrilla C, Viola RE. Characterization of human aspartoacylase: the brain enzyme responsible for Canavan disease. Biochemistry 2006;45:5878–5884. [PubMed: 16669630]

Le Moual H, Devault A, Roques BP, Crine P, Boileau G. Identification of glutamic acid 646 as a zinc-coordinating residue in endopeptidase-24.11. J Biol Chem 1991;266:15670–15674. [PubMed: 1678740]

Leone P, Janson CG, McPhee SJ, During MJ. Global CNS gene transfer for a childhood neurogenetic enzyme deficiency: Canavan disease. Curr Opin Mol Ther 1999;1:487–492. [PubMed: 11713764]

Madhavarao CN, Arun P, Moffett JR, et al. Defective N-acetylaspartate catabolism reduces brain acetate levels and myelin lipid synthesis in Canavan's disease. Proc Natl Acad Sci U S A 2005;102:5221–5226. [PubMed: 15784740]

Madhavarao CN, Hammer JA, Quarles RH, Namboodiri MA. A radiometric assay for aspartoacylase activity in cultured oligodendrocytes. Anal Biochem 2002;308:314–319. [PubMed: 12419345]

Makarova KS, Grishin NV. The Zn-peptidase superfamily: functional convergence after evolutionary divergence. J Mol Biol 1999;292:11–17. [PubMed: 10493853]

Matalon R, Kaul R, Michals K. Canavan disease: biochemical and molecular studies. J Inherit Metab Dis 1993;16:744–752. [PubMed: 8412017]

Matalon R, Michals-Matalon K. Recent advances in Canavan disease. Adv Pediatr 1999;46:493–506. [PubMed: 10645473]

Matalon R, Michals K, Kaul R. Canavan disease: from spongy degeneration to molecular analysis. J Pediatr 1995;127:511–517. [PubMed: 7562269]

Matalon R, Michals K, Sebesta D, Deanching M, Gashkoff P, Casanova J. Aspartoacylase deficiency and N-acetylaspartic aciduria in patients with Canavan disease. Am J Med Genet 1988;29:463–471. [PubMed: 3354621]

Medina JF, Wetterholm A, Radmark O, Shapiro R, Haeggstrom JZ, Vallee BL, Samuelsson B. Leukotriene A4 hydrolase: determination of the three zinc-binding ligands by site-directed mutagenesis and zinc analysis. Proc Natl Acad Sci U S A 1991;88:7620–7624. [PubMed: 1881903]

Mehta V, Namboodiri MA. N-acetylaspartate as an acetyl source in the nervous system. Brain Res Mol Brain Res 1995;31:151–157. [PubMed: 7476023]

Moore RA, Le Coq J, Faehnle CR, Viola RE. Purification and preliminary characterization of brain aspartoacylase. Arch Biochem Biophys 2003;413:1–8. [PubMed: 12706335]

Namboodiri MA, Corigliano-Murphy A, Jiang G, Rollag M, Provencio I. Murine aspartoacylase: cloning, expression and comparison with the human enzyme. Brain Res Mol Brain Res 2000;77:285–289. [PubMed: 10837925]

Olsen TR, Tranebjaerg L, Kvittingen EA, Hagenfeldt L, Moller C, Nilssen O. Two novel aspartoacylase gene (ASPA) missense mutations specific to Norwegian and Swedish patients with Canavan disease. J Med Genet 2002;39:e55. [PubMed: 12205125]

Qiao Y, Molina H, Pandey A, Zhang J, Cole PA. Chemical rescue of a mutant enzyme in living cells. Science 2006;311:1293–1297. [PubMed: 16513984]

Rees DC, Lewis M, Lipscomb WN. Refined crystal structure of carboxypeptidase A at 1.54 A resolution. J Mol Biol 1983;168:367–387. [PubMed: 6887246]

Rowsell S, Pauptit RA, Tucker AD, Melton RG, Blow DM, Brick P. Crystal structure of carboxypeptidase G2, a bacterial enzyme with applications in cancer therapy. Structure 1997;5:337–347. [PubMed: 9083113]

Shaag A, Anikster Y, Christensen E, et al. The molecular basis of canavan (aspartoacylase deficiency) disease in European non-Jewish patients. Am J Hum Genet 1995;57:572–580. [PubMed: 7668285]

Shoham G, Rees DC, Lipscomb WN. Effects of pH on the structure and function of carboxypeptidase A: crystallographic studies. Proc Natl Acad Sci U S A 1984;81:7767–7771. [PubMed: 6595659]

Sistermans EA, de Coo RF, van Beerendonk HM, Poll-The BT, Kleijer WJ, van Oost BA. Mutation detection in the aspartoacylase gene in 17 patients with Canavan disease: four new mutations in the non-Jewish population. Eur J Hum Genet 2000;8:557–560. [PubMed: 10909858]

Stenson PD, Ball EV, Mort M, Phillips AD, Shiel JA, Thomas NS, Abeysinghe S, Krawczak M, Cooper DN. Human Gene Mutation Database (HGMD): 2003 update. Hum Mutat 2003;21:577–581. [PubMed: 12754702]

Surendran S, Bamforth FJ, Chan A, Tyring SK, Goodman SI, Matalon R. Mild elevation of N-acetylaspartic acid and macrocephaly: diagnostic problem. J Child Neurol 2003a;18:809–812. [PubMed: 14696913]

Surendran S, Michals-Matalon K, Quast MJ, Tyring SK, Wei J, Ezell EL, Matalon R. Canavan disease: a monogenic trait with complex genomic interaction. Mol Genet Metab 2003b;80:74–80. [PubMed: 14567959]

Tacke U, Olbrich H, Sass JO, et al. Possible genotype-phenotype correlations in children with mild clinical course of Canavan disease. Neuropediatrics 2005;36:252–255. [PubMed: 16138249]

Vallee BL, Auld DS. Active-site zinc ligands and activated H2O of zinc enzymes. Proc Natl Acad Sci U S A 1990a;87:220–224. [PubMed: 2104979]

Vallee BL, Auld DS. Zinc coordination, function, and structure of zinc enzymes and other proteins. Biochemistry 1990b;29:5647–5659. [PubMed: 2200508]

Vazeux G, Wang J, Corvol P, Llorens-Cortes C. Identification of glutamate residues essential for catalytic activity and zinc coordination in aminopeptidase A. J Biol Chem 1996;271:9069–9074. [PubMed: 8621556]

Wouters MA, Husain A. Changes in zinc ligation promote remodeling of the active site in the zinc hydrolase superfamily. J Mol Biol 2001;314:1191–1207. [PubMed: 11743734]

Yalcinkaya C, Benbir G, Salomons GS, Karaarslan E, Rolland MO, Jakobs C, van der Knaap MS. Atypical MRI findings in Canavan disease: a patient with a mild course. Neuropediatrics 2005;36:336–339. [PubMed: 16217711]

Zafeiriou DI, Kleijer WJ, Maroupoulos G, Anastasiou AL, Augoustidou-Savvopoulou P, Papadopoulou F, Kontopoulos EE, Fagan E, Payne S. Protracted course of N-acetylaspartic aciduria in two non-Jewish siblings: identical clinical and magnetic resonance imaging findings. Brain Dev 1999;21:205–208. [PubMed: 10372908]

Zelnik N, Luder AS, Elpeleg ON, Gross-Tsur V, Amir N, Hemli JA, Fattal A, Harel S. Protracted clinical course for patients with Canavan disease. Dev Med Child Neurol 1993;35:355–358. [PubMed: 8335152]

Zeng BJ, Pastores GM, Leone P, Raghavan S, Wang ZH, Ribeiro LA, Torres P, Ong E, Kolodny EH. Mutation analysis of the aspartoacylase gene in non-Jewish patients with Canavan disease. Adv Exp Med Biol 2006;576:165–173. [PubMed: 16802711]discussion 361–163

Zeng BJ, Wang ZH, Ribeiro LA, et al. Identification and characterization of novel mutations of the aspartoacylase gene in non-Jewish patients with Canavan disease. J Inherit Metab Dis 2002;25:557–570. [PubMed: 12638939]

Abbreviations

CD
: Canavan disease

CNS
: central nervous system

ASPA
: aspartoacylase

NAA
: *N*-acetyl-L-aspartate

WT
: wild-type

ZnCPA
: zinc-dependent carboxypeptidase A

DMEM
: Dulbecco’s modified Eagle Medium

FBS
: fetal bovine serum

PBS
: phosphate buffered saline

pepASPA
: sera against a conserved ASPA peptide

α-βT
: monoclonal anti-β-tubulin antibody

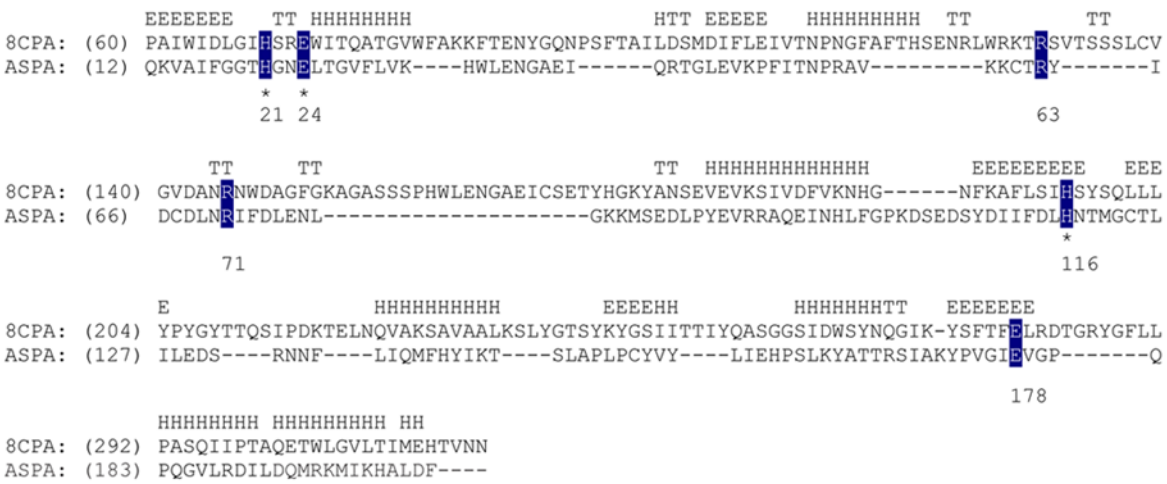

Fig 1. Sequence alignment between ASPA and bovine ZnCPA (PDB structure 8CPA)

The numbers indicated in parenthesis for the ASPA gene begin with the glutamine residue that aligns with proline 60 of ZnCPA. The conserved residues that are possibly involved in a zinc-dependent catalytic mechanism for ASPA are shown white in blue boxes with the putative zinc ligands highlighted by asterisks. The line above the alignment indicates the secondary structure (H for α-helix, E for extended, and T for turn) as reported with the 8CPA crystal structure (http://www.rcsb.org). Dashes denote amino acids that do not align with 8CPA. Residues predicted to be involved in catalysis are numbered below the alignment.

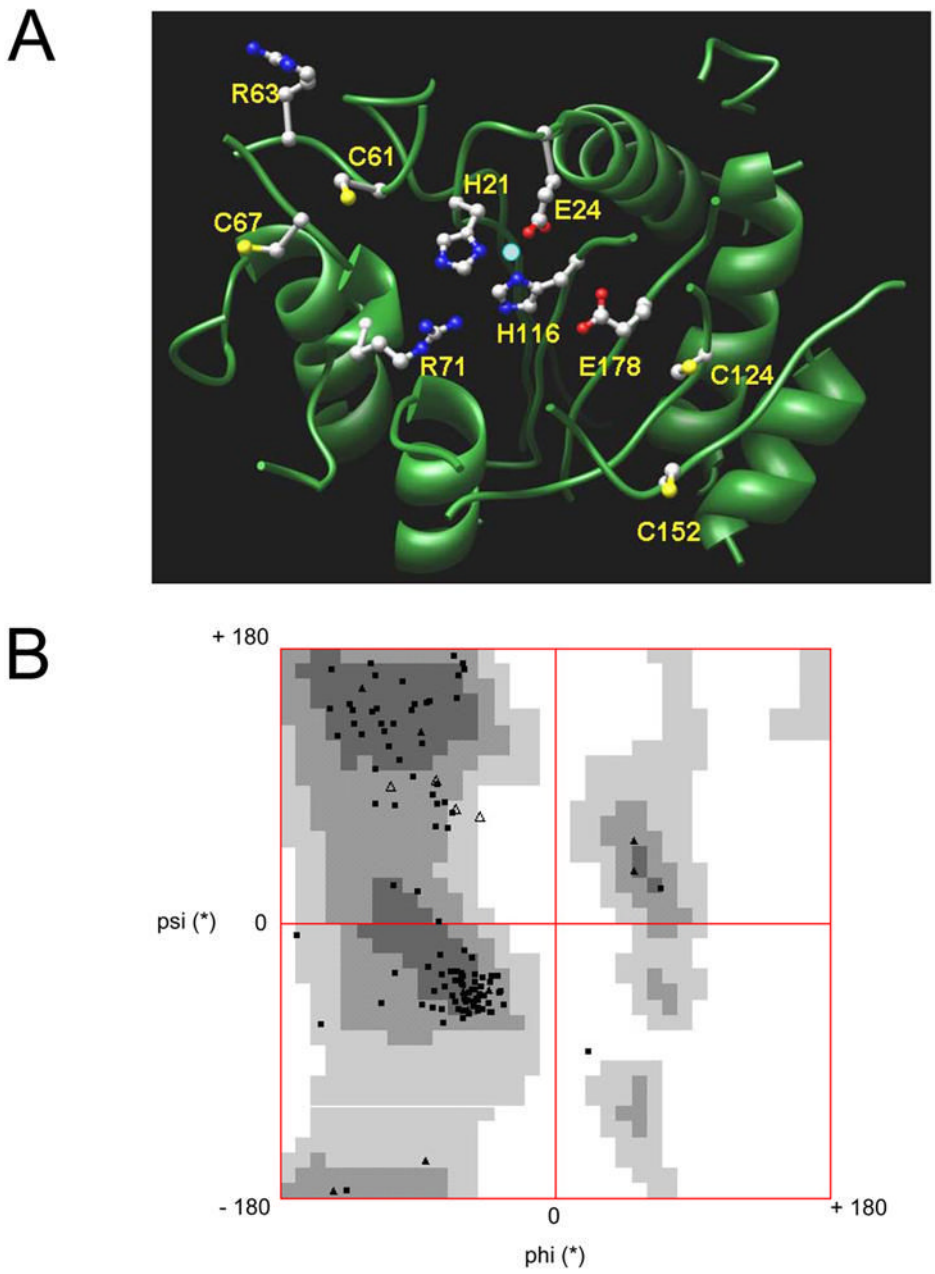

Fig 2. Partial 3D homology modeling of ASPA based on the crystal structure of bovine ZnCPA

A, The homology model for ASPA. Some of the loops are shown for clarity. The residues of interest in this report are depicted as ball-and-stick. A single zinc atom has been placed in the active site as a cyan sphere. *B*, Ramachandran Plot of the backbone torsion angles (phi and psi) for the homology model.

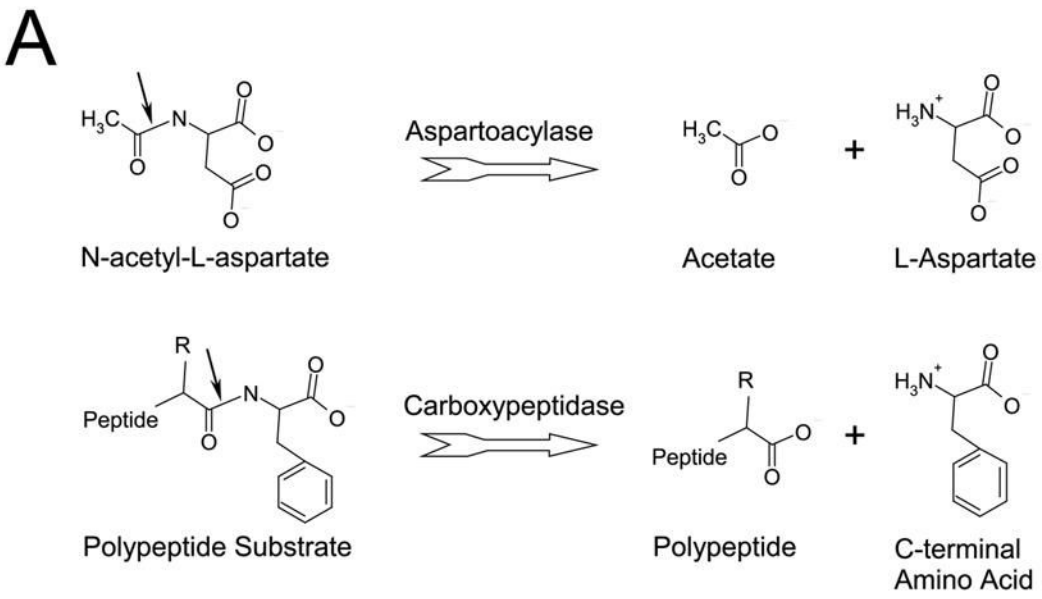

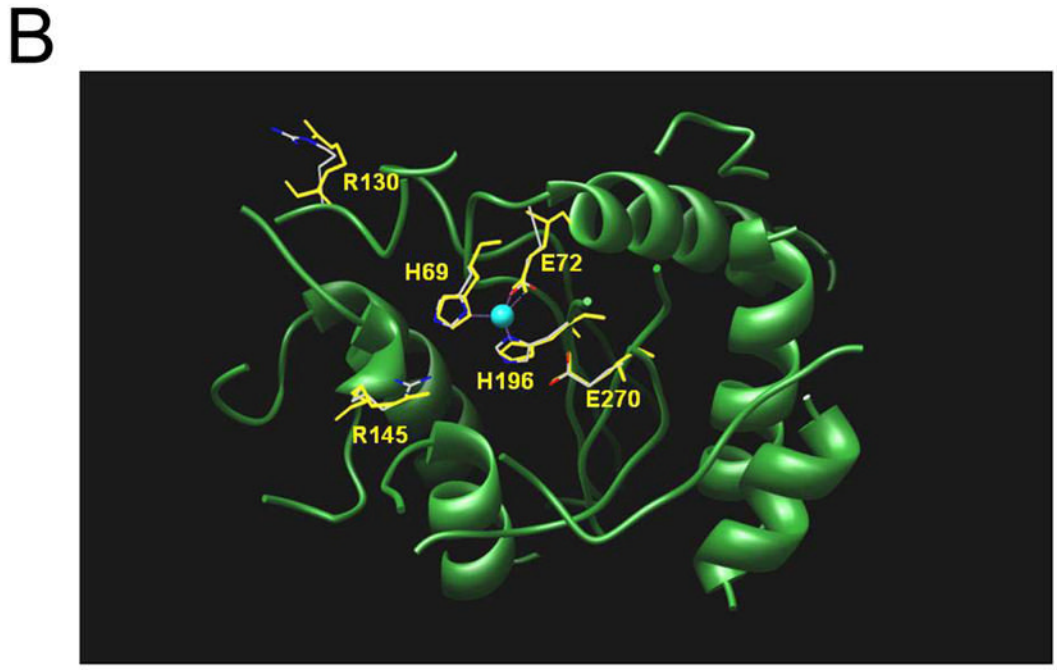

Fig 3. Comparison of reactions and active sites of ASPA and bovine ZnCPA

A, Chemical reactions catalyzed by ASPA and ZnCPA. The arrows point to hydrolyzed peptide bonds. *B*, Superposition of critical active site residues between ASPA and ZnCPA. The ASPA residues are depicted in atom color-coded ball-and-stick. The bovine ZnCPA residues are overlayed in thick yellow lines. Labeling corresponds to ZnCPA numbering.

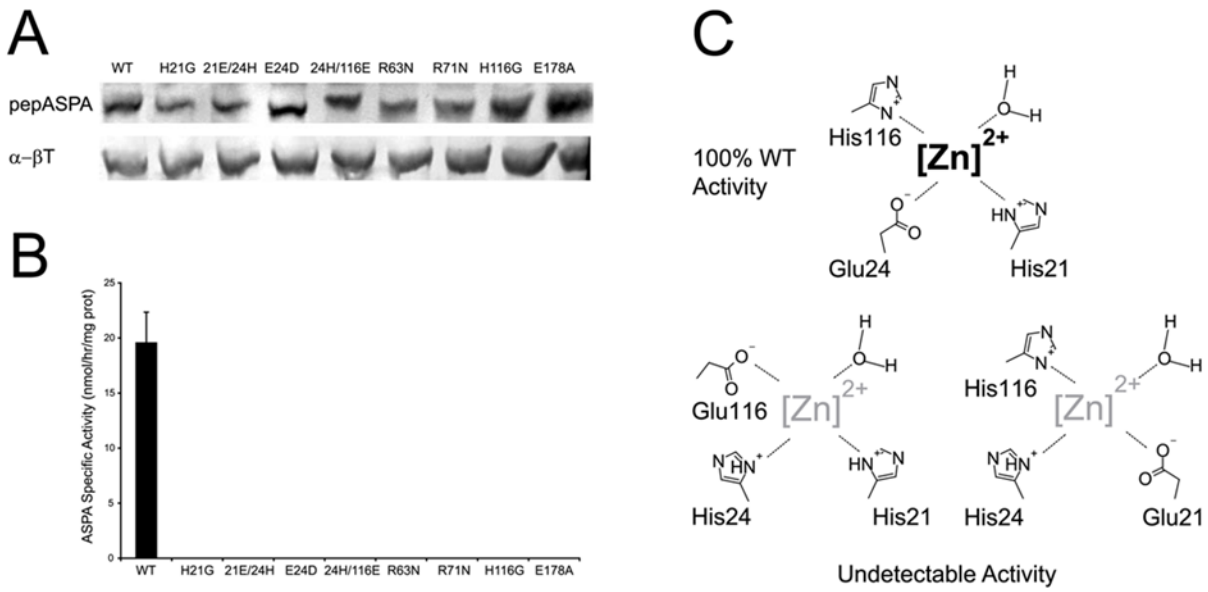

Fig 4. Mutational analysis of ASPA residues that align with those involved in bovine ZnCPA's catalytic mechanism

Whole cell extracts prepared from COS-7 cells transiently transfected with the indicated constructs were analyzed by immunoblotting and radiometric ASPA assay (see Materials and Methods). The enzyme activities are presented as mean +/− SEM for triplicate transfections. *A*, Immunoblotting using pepASPA and α-βT. *B*, Each putative catalytic mutation resulted in undetectable ASPA activity relative to WT. *C*, Changing the order of the putative Zn-binding ligands results in undetectable ASPA activity.

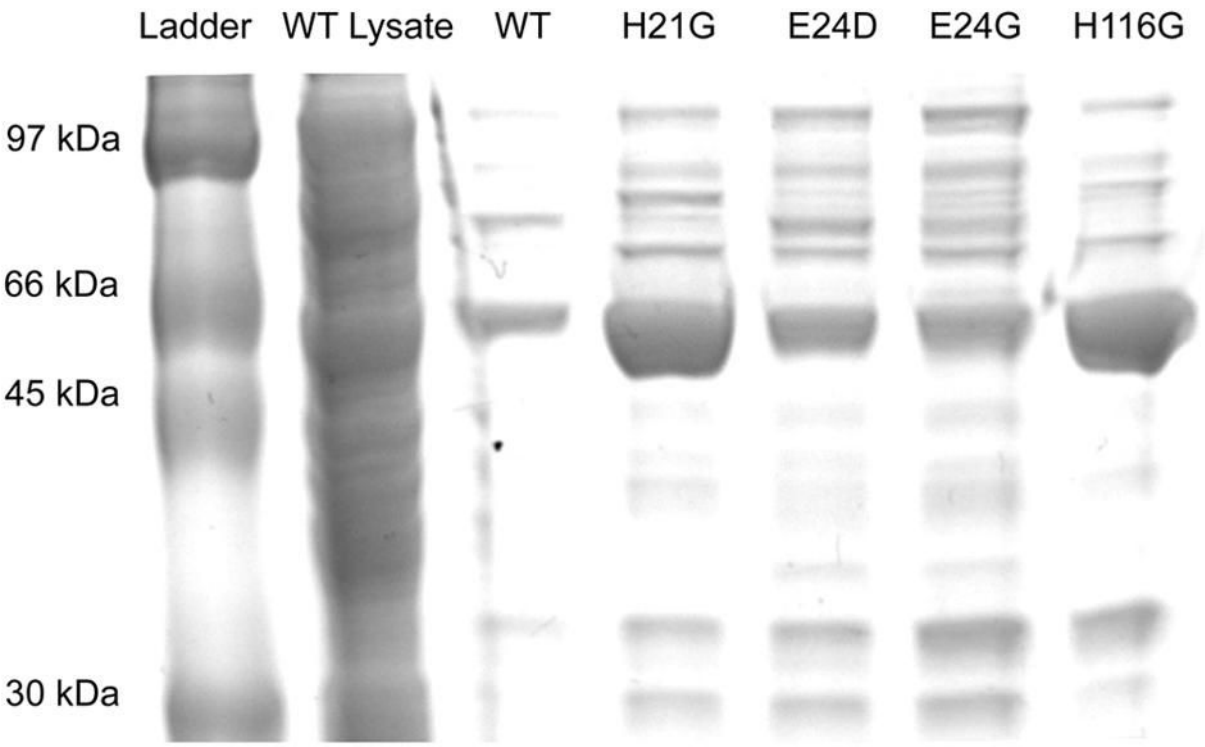

Fig 5. Purification of human ASPA from *E. coli*

The lysate and the indicated eluates of bacteria transformed with the indicated constructs were analyzed by SDS-PAGE and Coomassie staining (see Materials and Methods). Recombinant human ASPA fused to N-terminal thioredoxin and C-terminal V5 and (6x)-histidine tags was ~52 kDa.

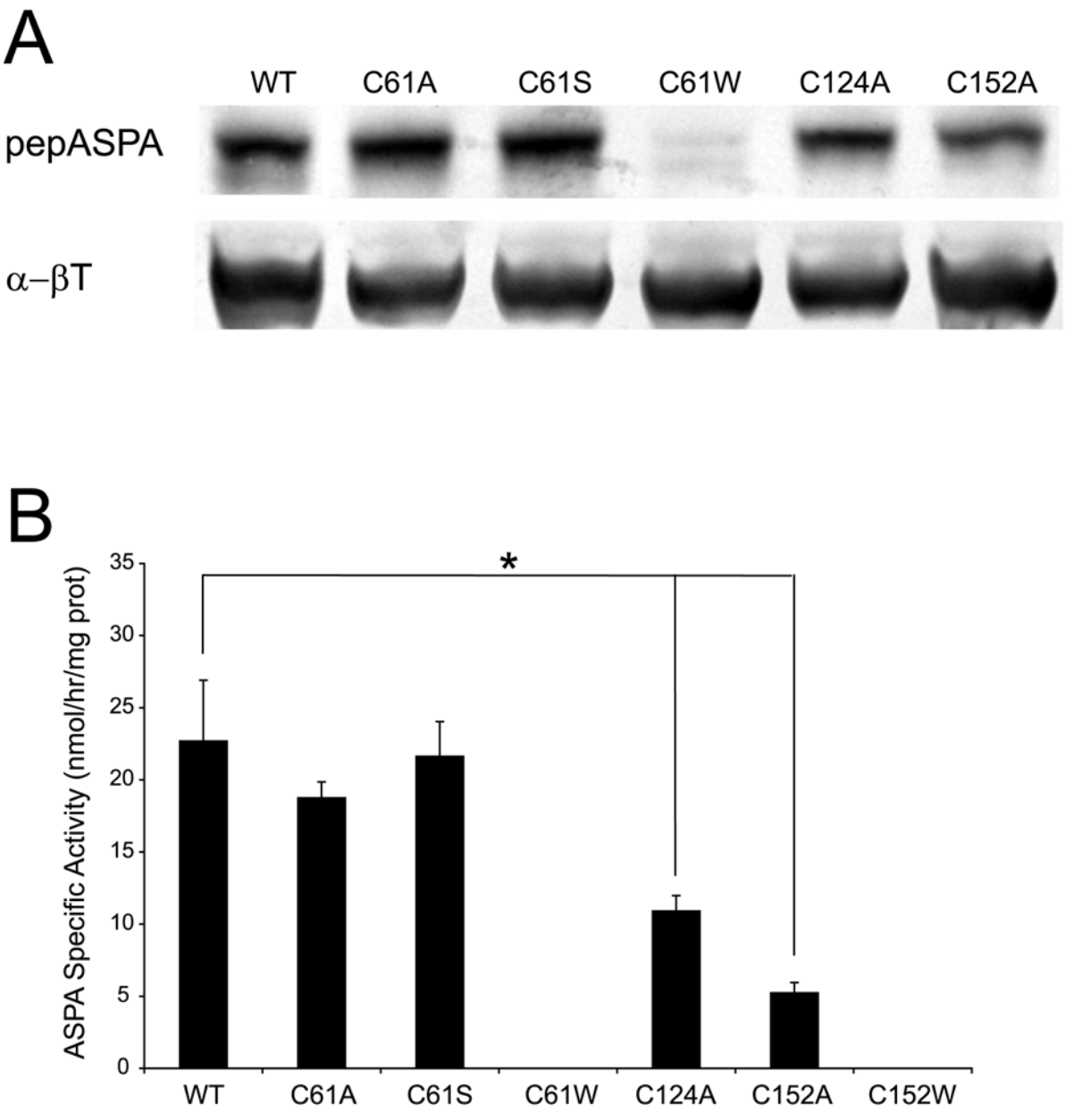

Fig 6. Cysteine mutational analysis indicates a possible disulfide bond in hASPA

Whole cell extracts prepared from COS-7 cells transiently transfected with the indicated constructs were analyzed by immunoblotting and radiometric ASPA assay (see Materials and Methods). The enzyme activities are presented as mean +/− SEM for six transfections. *A*, Immunoblotting using pepASPA and α-βT. *B*, Expression of C61A and C61S resulted in WT ASPA activity, expression of C124A and C152A resulted in statistically significantly reduced activity levels relative to WT (*; $p < 0.05$), and expression of C61W and C152W resulted in undetectable activity.

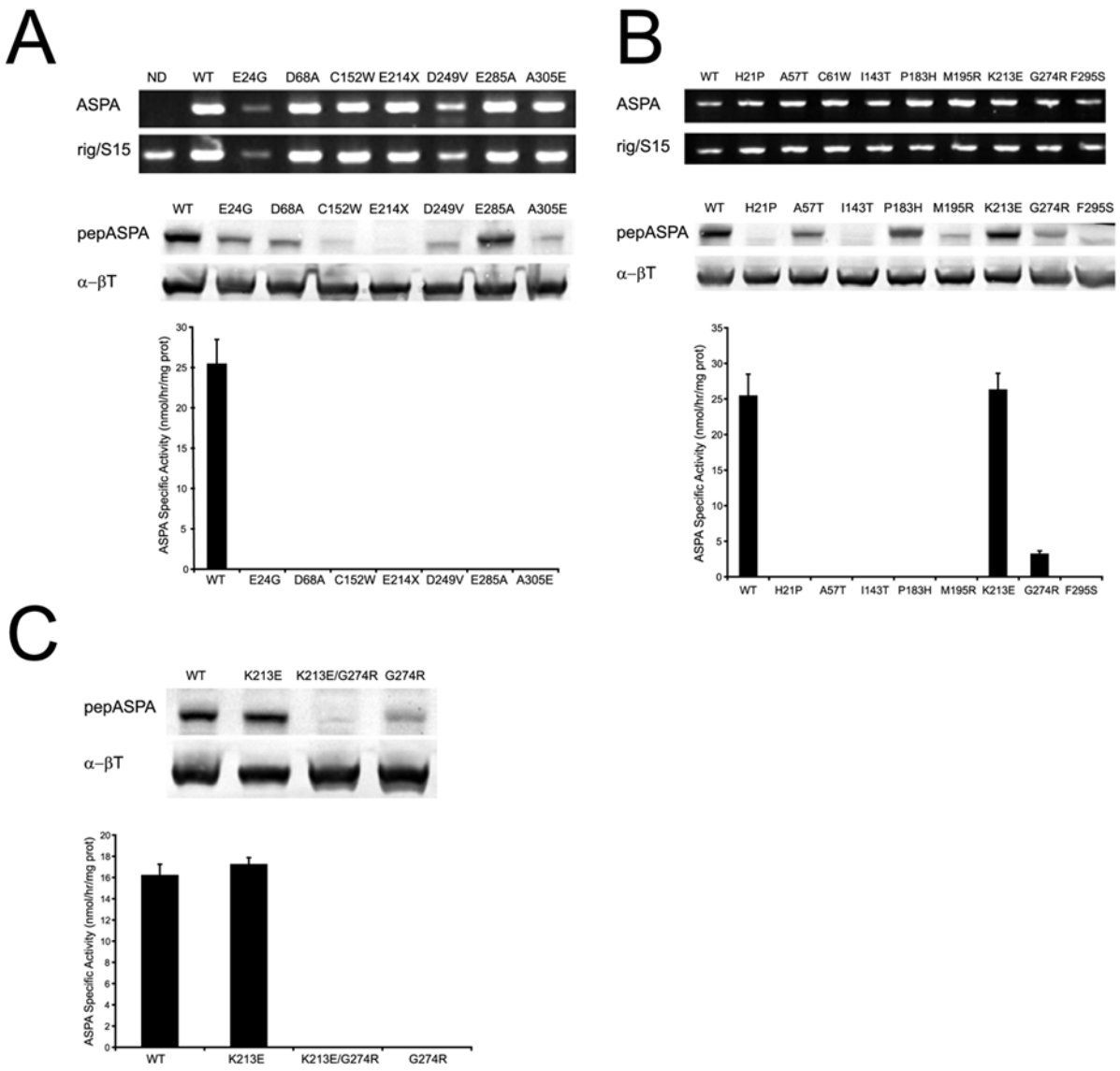

Fig 7. CD mutations give insight into hASPA structure

Whole cell extracts prepared from COS-7 cells transiently transfected with the indicated constructs were analyzed by immunoblotting and radiometric ASPA assay (see Materials and Methods). The enzyme activities are presented as mean +/− SEM for triplicate transfections. *ND*, No DNA mock transfection.. ***A,*** Analysis of select previously *in vitro* tested CD mutations. *Top panel:* RT-PCR confirmed that each mutant construct was expressed comparably to WT hASPA. *Middle panel:* Immunoblotting using a polyclonal peptide antibody (pepASPA) and β-tubulin loading control (α-βT). The ASPA band is 38 kDa and the beta-tubulin band is 50 kDa. *Bottom panel: In vitro* expression of each CD mutant resulted in undetectable ASPA activity compared to WT. ***B,*** Analysis of select previously *in vitro* untested CD mutations. *Top panel:* RT-PCR confirmed that each construct was expressed comparably to WT. *Middle panel:* Immunoblotting using pepASPA and α-βT. *Bottom panel:* Each mutant resulted in undetectable activity, with the following exceptions: WT activity for K213E and ~5% residual activity for G274R. *C,* Analysis of a case report of clinically mild CD. *Top panel:* Immunoblotting using pepASPA and α-βT. K213E/G274R is a double mutant expressed from a single plasmid (see Materials and Methods). *Bottom panel:* Expression of both G274R and

the K213E/G274R double mutant in this set of triplicate transfections resulted in undetectable ASPA activity compared to WT and K213E.

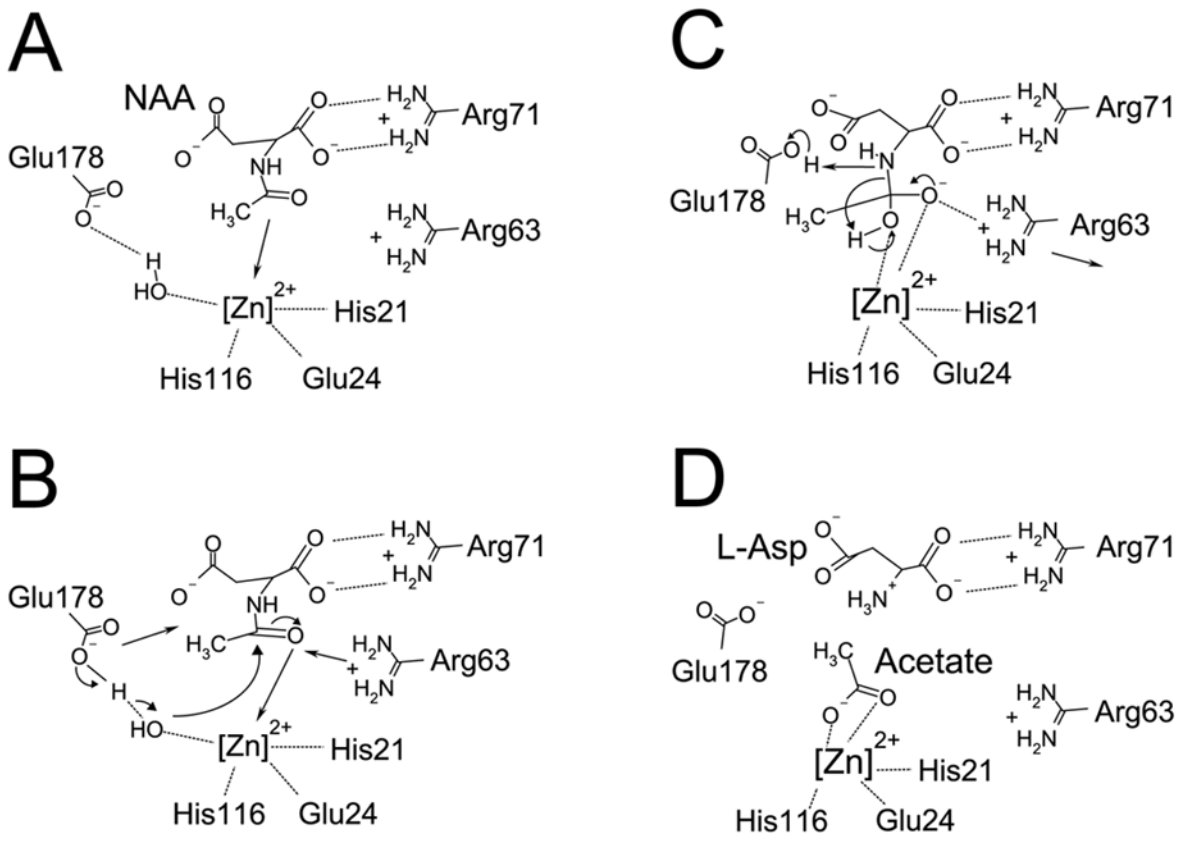

Fig 8. Proposed catalytic mechanism for NAA hydrolysis by ASPA

A, NAA substate binding. *B*, Nucleophilic attack. *C*, Transition state intermediate. *D*, Acetate and aspartate product formation.

Table 1

Mutational exploration of ASPA activity: rationale for selected residues

Zinc-Binding	Active Site and Catalysis	Non-Catalytic	C-Terminal CD Mutations
His21	Ala57	Ile143	Asp249
Glu24	Arg63	Cys152	Gly274
His116	Asp68	Met195	Glu285
	Arg71	Lys213	Phe295
	Glu178		Ala305
	Pro183		

Table 2

Summary table of CD missense mutations analyzed in this report.

DNA Mutation	Protein Mutation	Relative ASPA Activity	Ethnicity	Citations
A62C	H21P	Untested	Dutch	(Sistermans et al. 2000)
A71G	E24G	Undetectable	German	(Zeng et al. 2002)
G169A	A57T	Untested	German	(Sistermans et al. 2000)
A203C	D68A	Undetectable	British	(Zeng et al. 2002)
T428C	I143T	Untested	Japanese	(Kobayashi et al. 1998)
C456G	C152W	Undetectable	Yemenite	(Zeng et al. 2002)
C548A	P183H	Untested	French	(Elpeleg & Shaag 1999)
T584G	M195R	Untested	Algerian	(Elpeleg & Shaag 1999)
A637G	K213E	Untested	Greek	(Tacke et al. 2005)
A746T	D249V	Undetectable	British, Norwegian, Swedish	(Zeng et al. 2002,Olsen *et al.* 2002)
G820A	G274R	Untested	Turkish, Greek	(Elpeleg & Shaag 1999,Shaag et al. 1995,Tacke et al. 2005)
A854C	E285A	2.5%	Ashkenazi Jewish	(Kaul et al. 1994,Kaul et al. 1993,Kaul et al. 1996,Zeng et al. 2006,Zeng et al. 2002)
T884C	F295S	Untested	Greek, Turkish	(Elpeleg & Shaag 1999,Shaag et al. 1995,Tacke et al. 2005)
C914A	A305E	Undetectable	Pan-European	(Elpeleg & Shaag 1999,Janson et al. 2006,Kaul et al. 1994,Kaul et al. 1996,Shaag et al. 1995,Yalcinkaya et al. 2005,Zeng et al. 2006,Zeng et al. 2002)

ASPA activities relative to WT enzyme for CD mutations that have been previously recreated *in vitro* are listed.

Table 3

Table of forward primers used for site-directed mutagenesis of hASPA cDNA.

Amino Acid	Base Pair	Forward Mutagenic Primer
H21E/E24H	CAT61GAG, GAG70CAC	5′ GCTATCTTTGGAGGAACCGAGGGGAATCACCTAACCGG 3′
H21G	CA61GG	5′ CTATCTTTGGAGGAACCGGTGGGAATGAGCTAACCG 3′
H21P	A62C	5′ CTATCTTTGGAGGAACCCCTGGGAATGAGCTAACCG 3′
E24D	G72C	5′ GGAACCCATGGGAATGACCTAACCGGAGTATTTC 3′
E24G	A71G	5′ GGAACCCATGGGAATGGGCTAACCGGAGTATTTC 3′
E24H	GAG70CAC	5′ GGAGGAACCCATGGGAATCACCTAACCGGAGTATTTCTGG 3′
A57T	G169A	5′ CATTTATTACTAACCCCAGAACAGTGAAGAAGTGTACCAG 3′
C61A	TG181GC	5′ CCCAGAGCAGTGAAGAAGGCTACCAGATATATTGACTG 3′
C61S	T181A	5′ CCCAGAGCAGTGAAGAAGAGTACCAGATATATTGACTG 3′
C61W	T183G	5′ CAGAGCAGTGAAGAAGTGGACCAGATATATTGACTGTG 3′
R63N	GA188AC	5′ GAGCAGTGAAGAAGTGTACCAACTATATTGACTGTGACCTG 3′
D68A	A203C	5′ CCAGATATATTGACTGTGCCCTGAATCGCATTTTTGAC 3′
R71N	CG211AA	5′ CCAGATATATTGACTGTGACCTGAATAACATTTTTGACCTTGAAAATCTTGGC 3′
H116E	CAC346GAG	5′ CTATGACATTATTTTTGACCTTGAGAACACCACCTCTAACATGGGGTG 3′
H116G	CA346GG	5′ CTATGACATTATTTTTGACCTTGGCAACACCACCTCTAACATGGG 3′
C124A	TG370GC	5′ CCACCTCTAACATGGGGGCCACTCTTATTCTTGAGG 3′
I143T	T428C	5′ CTTTTTAATTCAGATGTTTCATTACACTAAGACTTCTCTGGCTCCACTACCC 3′
C152A	TG454GC	5′ CTCTGGCTCCACTACCCGCCTACGTTTATCTGATTG 3′
C152W	C456G	5′ CTGGCTCCACTACCCTGGTACGTTTATCTGATTG 3′
E178A	A533C	5′ GTATCCTGTGGGTATAGCAGTTGGTCCTCAGCCTC 3′
P183H	C548A	5′ GAAGTTGGTCCTCAGCATCAAGGGGTTCTGAG 3′
M195R	T584G	5′ GAGAGCTGATATCTTGGATCAAAGGAGAAAAATGATTAAACATGCTC 3′
D204H	G610C	5′ CAAATGAGAAAAATGATTAAACATGCTCTTCATTTTATACATCATTTCAATGAAGGAAAAG 3′
K213E	A637G	5′ CATCATTTCAATGAAGGAGAAGAATTTCCTCCCTGCGC 3′
E214X	G640T	5′ CATTTCAATGAAGGAAAATAATTTCCTCCCTGCGCC 3′
D249V	A746T	5′ CCATCCTAATCTGCAGGTTCAAGACTGGAAACCAC 3′
G274R	G820A	5′ GACGATCCCACTGGGCAGAGACTGTACCGTGTAC 3′
E285A	A854C	5′ GTACCCCGTGTTTGTGAATGCGGCCGCATATTACGAAAAG 3′
F295S	T884C	5′ CATATTACGAAAAGAAAGAAGCTTCTGCAAAGACAACTAAACTAACGC 3′
A305E	C914A	5′ CTAAACTAACGCTCAATGAAAAAAGTATTCGCTGCTG 3′